THE JOURNAL OF PHYSICAL CHEMISTRY A
A JOURNAL OF THE AMERICAN CHEMICAL SOCIETY

Article

Directed Gas-Phase Formation of the 1-Cyanovinyl Radical (H_2CCCN, X^2A') in the Interstellar Medium

Shane J. Goettl,[#] Ashleigh G. Hartwig,[#] Zhenghai Yang, Alexander M. Mebel,* and Ralf I. Kaiser*

Cite This: *J. Phys. Chem. A* 2026, 130, 242−249

Read Online

ACCESS | Metrics & More | Article Recommendations | Supporting Information

ABSTRACT: The formation pathways to nitrogen-containing molecules and radicals are crucial to the understanding of the carbon−nitrogen chemistry in interstellar and atmospheric environments. While over 65 nitrogen-containing neutral species have been observed in deep space to date, their formation mechanisms—in particular, those of radical species—remain largely speculative. The crossed molecular beam technique in conjunction with electronic structure and statistical calculations was utilized to offer a detailed overview of the fundamental pathways in the gas-phase bimolecular reaction of ground-state atomic carbon (C, ^3P) with acetonitrile-d_3 (CD_3CN, X^1A_1) under single-collision conditions leading to the formation of the 1-cyanovinyl radical (D_2CCCN, X^2A') coupled with deuterium atom loss. The indirect reaction was initiated by barrierless carbon-atom addition, with the most probable route involving carbon addition across the carbon−nitrogen nitrile triple bond of acetonitrile, forming a three-membered ring intermediate followed by ring-opening and unimolecular decomposition via atomic deuterium loss from the C3 carbon atom. The reaction was overall exoergic, and intermediates and transition states lie lower in energy than the separated reactants, unlocking the reaction of carbon with acetonitrile in low-temperature environments such as cold molecular clouds, e.g., Taurus Molecular Cloud (TMC-1), and planetary atmospheres, e.g., Saturn's moon Titan. In these environments, the 1-cyanovinyl radical may act as a building block for cyano-substituted polycyclic aromatic hydrocarbons and N-heterocycles, thus furthering our understanding of the complex carbon−nitrogen chemistry in deep space.

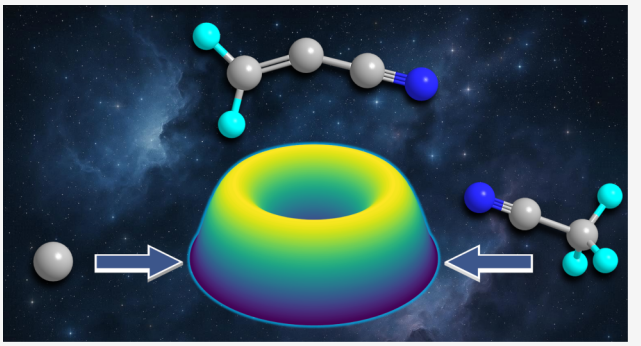

1. INTRODUCTION

Since the first observation of the cyano radical (CN, $X^2\Sigma^+$) toward ζ Ophiuchi more than 80 years ago,[1] multiple nitrogen-containing molecules such as nitriles,[2] amines,[3] and imines[4] have been discovered in various astrophysical regions, with particular interest directed to cold molecular clouds such as TMC-1 and the atmospheres of planetary bodies like Saturn's moon Titan.[5−8] In the last few years alone, the list of detected molecules in the ISM has nearly doubled, with over 65 observed neutral compounds containing (iso)cyano moieties thus far.[9] Simple nitriles such as hydrogen cyanide (HCN),[10] acetonitrile (CH_3CN),[11] and vinylcyanide (CH_2CHCN)[12] are ubiquitous throughout deep space and easily detected via microwave spectroscopy due to their large dipole moments. While the dehydrogenated radicals of hydrogen cyanide (cyano, CN) and acetonitrile (cyanomethyl, CH_2CN) were observed decades ago,[1,13] only recently has the 1-cyanovinyl radical (H_2CCCN)—the singly dehydrogenated radical counterpart of vinylcyanide—been identified in the Taurus Molecular Cloud (TMC-1),[14] while the *Z*- and *E*-2-cyanovinyl isomers—along with the isocyanovinyl counterparts—remain elusive. Astrochemical models predict that the reaction of carbon atoms with acetonitrile is the most favored pathway to the 1-cyanovinyl radical, whereas the atomic nitrogen reaction with propargyl (CH_2CCH) should also contribute to a lesser extent.[14] The kinetics of the C/CH_3CN system to the 1-cyanovinyl radical coupled with atomic hydrogen loss have been previously elucidated,[15] showing fast rate constants of $(3−4) \times 10^{-10}$ cm^3 s^{-1}; however, a detailed mechanistic and dynamic study under single-collision conditions is still lacking.

The molecular structures of the 1-cyanovinyl radical and the 2-cyanovinyl isomers are shown in Figure 1.[16,17] The greater stability of the 1-cyanovinyl radical of 28 kJ mol^{-1} compared with its isomers may be due to resonance stabilization within the C_3N backbone, which is absent in *Z*- and *E*-2-cyanovinyl radicals. Perhaps due in part to the resonance stabilization, the carbon chain within 1-cyanovinyl features a C−C−C bond angle of 152°, while the 2-isomers have molecular structures more similar to vinylcyanide with C−C−C bond angles of 122−123°. Further insight into the molecular properties and

Published: December 26, 2025

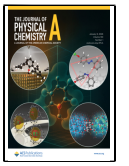

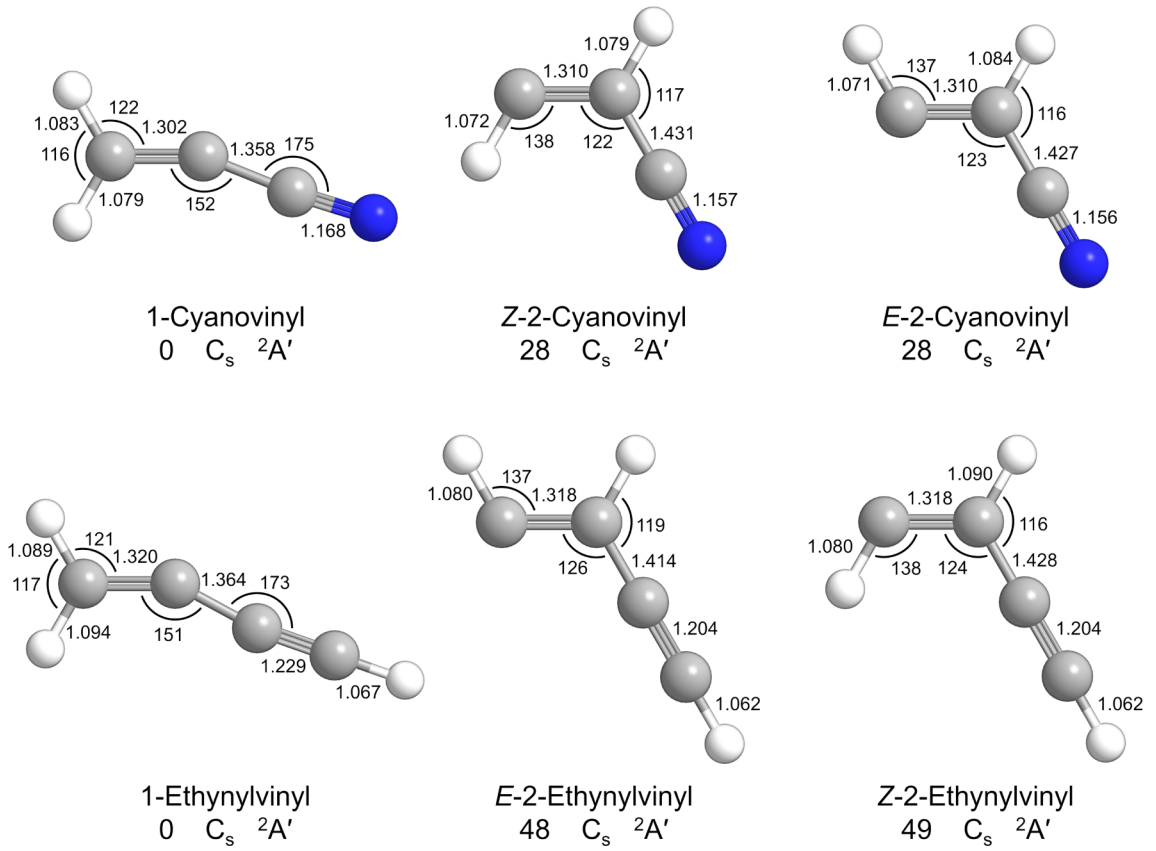

Figure 1. Structures of the C_3NH_2 isomers and the isovalent C_4H_3 species. Relative energies between isomers are given in kJ mol^{-1}, bond angles in degrees, and bond lengths in angstroms. Point groups and electronic ground-state term symbols are also shown. Carbon atoms are denoted in gray, nitrogen atoms in blue, and hydrogen atoms in white.

chemical bonding is often obtained by comparison with isovalent species; in this case, the ethynylvinyl radical (C_4H_3) with its three most stable structures.[18,19] As shown in Figure 1, the cyanovinyl and ethynylvinyl radicals are nearly identical with respect to bond lengths and angles. The energy gap between the 1- and 2-structures provides the largest difference, with the ethynylvinyl gap about 20 kJ mol^{-1} greater than the energy gap for cyanovinyl. While the more stable 2-isomer is calculated to be *Z* for cyanovinyl and *E* for ethynylvinyl, the energies between the *E* and *Z* configurations are so close as to be effectively the same within the error bars of the calculations. Previous studies on the reaction of ground-state atomic carbon with methylacetylene (CH_3CCH)[18] and allene (H_2CCCH_2)[20] revealed the formation of the 1-ethynylvinyl radical along with atomic hydrogen loss, which further reinforces the prediction of the isovalent 1-cyanovinyl radical formation from the nitrogen-containing equivalent reaction of atomic carbon with acetonitrile.

Herein, we report on the gas-phase reaction of ground-state atomic carbon (C, ^3P) with acetonitrile-d_3 (CD_3CN) under single-collision conditions by utilizing the crossed molecular beam technique coupled with electronic structure and statistical calculations. The reaction may proceed through multiple barrierless entrance channels featuring carbon atom addition to the carbon of the cyano group, the nitrogen of the cyano group, or across the carbon−nitrogen triple bond of the cyano group, eventually leading via ring-closing and opening isomerization to the 1-cyanovinyl radical (D_2CCCN, X^2A') coupled with atomic deuterium loss in an overall exoergic reaction. Both reactants are common in extraterrestrial sources. Since there is no entrance barrier and all intermediates and transition states lie lower in energy than the separated reactants, the reaction of carbon with acetonitrile can proceed rapidly to the 1-cyanovinyl radical in low-temperature environments such as cold molecular clouds, e.g., TMC-1, and planetary atmospheres, e.g., Saturn's moon Titan, where temperatures can get as low as 10 K[21] and 70 K,[22] respectively.

2. METHODS

2.1. Experimental Methods. The reaction of ground-state atomic carbon (C, ^3P) with acetonitrile-d_3 (CD_3CN, X^1A_1, 99.9%, Sigma-Aldrich) was conducted under single-collision conditions utilizing a crossed molecular beams apparatus.[23] Carbon atoms were generated *in situ* from laser ablation of a rotating graphite rod using the fourth harmonic (266 nm) output of an Nd:YAG laser (Quanta-Ray Pro 270, Spectra-Physics) operating at 30 Hz and 8−12 mJ per pulse focused to a spot size of less than 1.5 mm^2. Helium (He, 99.9999%, Airgas) was pulsed through a Proch−Trickl[24] valve at a backing pressure of 4 atm, amplitude of −400 V, 60 Hz frequency, and pulse width of 80 μs before carrying the ablated carbon atoms through a 1 mm diameter skimmer and attaining supersonic expansion. A chopper wheel selected a carbon peak velocity (v_p) of 2298 ± 67 m s^{-1} and a speed ratio (S) of 2.6 ± 0.2. A second molecular beam was generated by sending argon (Ar, 99.9999%, Airgas) at a backing pressure of 550 Torr through a stainless-steel bubbler containing acetonitrile-d_3 (purified by multiple freeze−pump−thaw cycles) and pulsing the resulting gas mixture through a pulsed valve (−350 V, 60

https://doi.org/10.1021/acs.jpca.5c07260
J. Phys. Chem. A 2026, 130, 242−249

Hz, 80 μs) and skimmer. In the interaction region, the carbon beam crossed the acetonitrile-d_3 beam (v_p = 710 ± 6 m s^{-1}, S = 11.6 ± 1.7) giving a collision energy (E_C) of 27.3 ± 1.5 kJ mol^{-1} and center-of-mass angle (Θ_{CM}) of 49.3 ± 1.1°. It should be noted that dicarbon (C_2, $X^1\Sigma_g^+/a^3\Pi_u$) and tricarbon (C_3, $X^1\Sigma_g^+$) molecules were also produced in the ablation source at minor levels of less than a few percent. However, the signal recorded at m/z = 52 and 54 can only be replicated with a single channel via the reaction of atomic carbon with acetonitrile-d_3 (Section 3).

Reactive scattering products were collected by a triply differentially pumped universal detector, which can rotate within the plane of the reactant beams. Products that entered the detector were ionized by electron impact ionization at 80 eV and filtered by mass-to-charge ratio (m/z) with a quadrupole mass spectrometer (150QC, Extrel) operating in the time-of-flight (TOF) mode. Signal acquisition and enhancement were performed with a Daly-type setup.[25] Up to 5.4 × 10^6 TOFs in an angular range of 9.3° ≤ Θ ≤ 64.3° were scanned in 5° steps, where 0° is defined by the carbon beam and 90° corresponds to the acetonitrile-d_3 beam. Integrating the TOFs at each angle and normalizing to Θ_{CM} provides a laboratory angular distribution (LAD). Additional chemical dynamics information was acquired by using a forward convolution routine to fit the laboratory data with user-defined CM translational energy ($P(E_T)$) and angular ($T(\theta)$) flux distributions.[26,27] Briefly, the $P(E_T)$, or kinetic energy release probability distribution, during the decomposition of an intermediate to products can often be given by the following:

$$P(E_T) = (E_T - B)^p (D - E_T)^q$$

where B, D, p, and q are varied to alter the shape of the $P(E_T)$. Likewise, the $T(\theta)$ is approximated by a sum of Legendre's polynomials $L_i(\cos\theta)$ with a_i coefficients:

$$T(\theta) = \sum_{i=0}^{n} a_i L_i(\cos\theta)$$

Because products are scattered with cylindrical symmetry about the products' relative velocity vector, the $T(\theta)$ is only shown from 0° to 180°. A CM flux contour map can then be defined:

$$I(u, \theta) \approx P(u)T(\theta)$$

where $I(u, \theta)$ is the reaction differential cross section and $P(u)$ is the product velocity distribution in the CM frame determined from E_T. The laboratory data fitting routine utilizes the relation between the measured TOFs, $N(\Theta, t)$, and the CM distributions, $P(E_T)$ and $T(\theta)$, as given by

$$N(\Theta, t) = CT(\theta)P(E_T)\frac{v^3}{u}$$

where v and u are the laboratory and CM product velocities, respectively, and C is a constant. More details on the lab-to-CM transformation are found in ref 28.

2.2. Computational Methods. Theoretical calculations were carried out with the GAUSSIAN 16 software package[29] available through Florida International University's High-Performance Computing (HPC) facility from the Instructional and Research Computing Center (IRCC). The geometries of all species (including reactants, products, intermediates, and transition states) in the reaction of ground-state atomic carbon (C, ^{3}P) with acetonitrile (CH_3CN, X^1A_1) were optimized using the density functional theory (DFT) ωB97XD functional and the 6-311G** basis set. The ωB97XD functional, which incorporated empirical dispersion corrections, generally yielded more compact geometries and more accurate bond lengths than older functionals such as B3LYP, which often overestimated internuclear distances.[30,31] The 6-311G** refers to six primitive Gaussian functions specific to the core electrons and three basis functions for each valence orbital contracted as 311 in terms of primitive Gaussian functions. The two asterisks represent the addition of polarization functions (d functions for sp-elements like C and N and p functions for the hydrogens), allowing for more flexibility in the electron density clouds. Vibrational frequencies were computed for all optimized structures at the same ωB97XD/6-311G** level of theory and were utilized to evaluate zero-point vibrational energy corrections (ZPE) and for rate constant calculations (*vide infra*). Single-point energies of each of the stationary points on the investigated potential energy surface (PES) were refined using the explicitly correlated coupled-cluster method with single and double excitation, as well as the perturbation theory treatment of triple excitations, CCSD(T)-F12/cc-pVQZ-F12/cc-pVQZ-F12, as implemented in MOLPRO 2021,[32] which approached the complete basis set limit (CBS) and gave a more accurate representation of the relative energies for all species involved in the reactions. The mean average error is expected to be typically within 2−4 kJ mol[33] when the more accurate CCSD(T)-F12/cc-pVQZ-F12 level of theory was used.

The energy-dependent rate constants of the unimolecular reaction steps were calculated using the Rice−Ramsperger−Kassel−Marcus (RRKM) theory.[34,35] This theory utilized parameters from the PES to determine the rate of all unimolecular reaction steps as a function of the reactant's energy as the energized reactant isomerized and/or dissociated.[36] Product branching ratios were computed at the zero-pressure limit corresponding to experimental single-collision conditions by using the steady-state approximation. At such conditions, master equations for unimolecular reactions can be expressed as follows:

$$\frac{d[C]_i}{dt} = \sum k_n[C]_j - \sum k_m[C]_i$$

with $[C]_i$ and $[C]_j$ being concentrations of various intermediates or products and k_n and k_m being microcanonical rate constants for the production and consumption of an intermediate C_i computed within the RRKM theory. Only a single total energy level was considered throughout, as at the zero-pressure limit, where the available internal energy of each intermediate was assumed to be equal to the sum of the collision energy and the energy of chemical activation, which, in turn, is equal to the negative of the relative energy of the species with regard to the C(^{3}P) + CH_3CN reactants. As rate constants of different unimolecular reaction steps are independent of each other, relative product yields can be determined from the solution of the system of coupled master equations. Within the steady-state approximation, this system of differential equations is reduced to a system of linear equations where the concentration of a chosen initial intermediate formed in the bimolecular reaction is taken as a constant and concentrations of all other unimolecular intermediates remain steady, so that their $\frac{d[C]_i}{dt} = 0$. We

https://doi.org/10.1021/acs.jpca.5c07260
J. Phys. Chem. A 2026, 130, 242−249

employed our internal UNIMOL code[37,38] to compute the rate constants and product branching ratios. UNIMOL postprocesses GAUSSIAN log files to extract molecular parameters of intermediates and transition states, including rotational constants and vibrational frequencies, calculates energy-dependent rate constants for the entire user-specified unimolecular reaction network within the rigid-rotor harmonic oscillator (RRHO) approximation, and then solves the steady-state equations to obtain product branching ratios given the initial intermediate produced in the entrance channel of the bimolecular reaction.

3. RESULTS AND DISCUSSION

3.1. Laboratory Frame. For the reaction of carbon with acetonitrile-d_3, reactive scattering TOF spectra were collected at Θ_{CM} for m/z = 54 ($C_3ND_2^+$) and 52 (C_3ND^+). These TOFs overlap after scaling (Figure S1) indicating that the signal at m/z = 52 originates from fragmentation by the electron impact ionizer of atomic deuterium loss products seen at m/z = 54. No signal was observed for the adduct at m/z = 56. The signal-to-noise ratio at m/z = 52 was larger than that at m/z = 54; therefore, the LAD (Figure 2a) was collected using the former m/z. Six representative TOFs taken at distinct angles are shown in Figure 2b, which feature a sharp rise and a gradual decline with total widths of about 500 μs. The LAD is forward−backward symmetric with respect to Θ_{CM}, which implies that the reaction of carbon with acetonitrile-d_3 progresses through C_3ND_3 intermediate(s) in overall indirect mechanism(s) eventually producing C_3ND_2 product(s) coupled with atomic deuterium loss (Reaction 1).

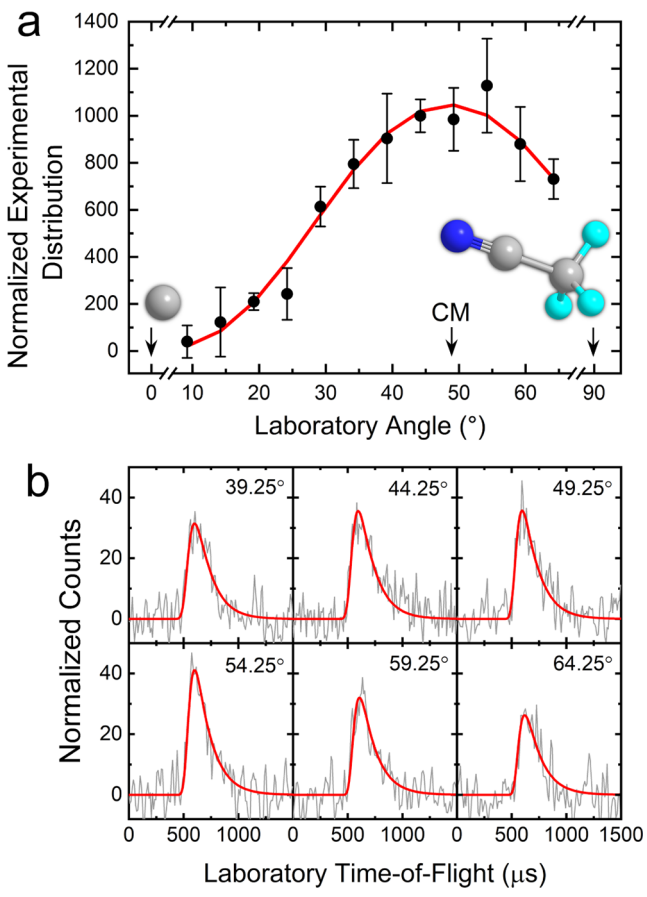

Figure 2. Laboratory angular distribution (a) and time-of-flight (TOF) spectra (b) recorded at mass-to-charge (m/z) = 52 for the reaction of carbon (C, ^{3}P) with acetonitrile-d_3 (CD_3CN) conducted at a collision energy of 27.3 ± 1.5 kJ mol^{-1}. CM represents the center-of-mass angle, and 0° and 90° define the directions of the carbon and acetonitrile-d_3 beams, respectively. The black circles depict the data, and the red lines represent the fits. Carbon atoms are colored gray, nitrogen atoms blue, and deuterium atoms cyan.

$$C\ (12\ amu) + CD_3CN\ (44\ amu) \rightarrow C_3ND_2\ (54\ amu) + D\ (2\ amu) \quad (1)$$

$$C\ (12\ amu) + CD_3CN\ (44\ amu) \rightarrow C_3ND\ (52\ amu) + D_2\ (4\ amu) \quad (2)$$

3.2. Center-Of-Mass Frame. To acquire additional information about the reaction dynamics, the laboratory data were transformed to the CM frame of reference (Section 2). The laboratory data could be fit with a single reaction channel corresponding to atomic deuterium loss, forming C_3ND_2 product(s). First, $P(E_T)$ features a threshold (E_{max}) at 181 ± 17 kJ mol^{-1} (Figure 3a). Conservation of energy dictates that the reaction energy is equal to the difference in E_C and E_{max} for products without internal excitation; this provides a reaction energy of −154 ± 19 kJ mol^{-1}. In addition, the $P(E_T)$ peaks at 46 ± 5 kJ mol^{-1}, indicating that the title reaction proceeds through an exit channel with a tight transition state and hence considerable electron rearrangement prior to product formation.[39] This is most clearly explained by visualizing the reverse reaction. If the intermediate decomposing to products has an exit barrier, i.e., an activation barrier in the reverse reaction, then some or all of the reverse activation energy is converted to kinetic energy of the products resulting in the most probable kinetic energy release peaking away from zero. Second, the $T(\theta)$ shows an isotropic distribution with equal intensity at all angles (Figure 3b). This reveals that the reactants' collision forms intermediate(s) that have long lifetime(s) such that multiple rotational periods occur, resulting in deuterium atom ejection in a random direction; hence, scattering probability is equal for all angles. This reinforces the conclusion that the C/CD_3CN system progresses through an indirect reaction mechanism, since direct reactions feature strong forward or backward scattering of products giving asymmetric angular distributions. The "flat" distribution results from a poor coupling between the initial and final angular momenta with most of the kinetic energy released into the light deuterium atom.[40] Finally, utilizing both the $P(E_T)$ and $T(\theta)$, the flux contour map highlights the overall outcome of the reaction (Figure 3c).

3.3. Potential Energy Surface. To understand the mechanisms involved and the nature of the intermediate(s) and product(s), the experiments were combined with high-level electronic structure calculations, which are visualized in Figure 4 as a PES. All reactants, intermediates, transition states, and products were calculated at the CCSD(T)-F12/cc-pVQZ-F12//ωB97XD/6-311G** + ZPE(ωB97XD/6-311G**) level of theory, providing expected accuracies of ±2 to 4 kJ mol^{-1}. The experimentally derived reaction energy of −154 ± 19 kJ mol^{-1} matches the calculated reaction energy of the 1-cyanovinyl radical (H_2CCCN, **p1**) of −152 kJ mol^{-1}, while the next most stable products—the *Z*- and *E*-2-cyanovinyl isomers (HCCHCN, **p2**/**p2′**)—and the isocyanovinyl counterparts (**p3**, **p4**, **p4′**) lie outside the experimental energy error bars.

https://doi.org/10.1021/acs.jpca.5c07260
J. Phys. Chem. A 2026, 130, 242−249

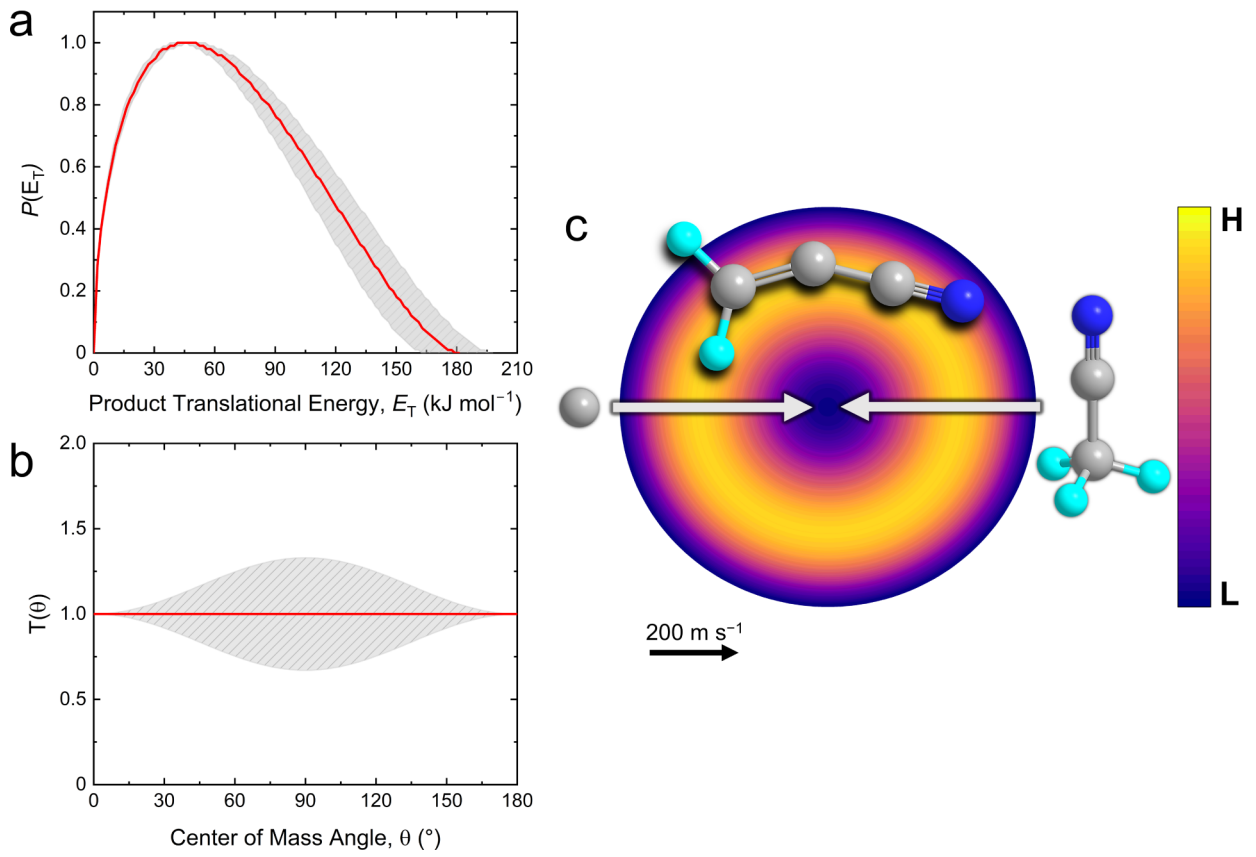

Figure 3. CM product translational energy (a) and angular (b) flux distribution, as well as the associated flux contour map (c) leading to the formation of C_3ND_2 product(s) in the reaction of carbon (C, ^3P) with acetonitrile-d_3 (CD_3CN) conducted at a collision energy of 27.3 ± 1.5 kJ mol^{-1}. Red lines define the best-fit functions, while shaded areas provide the error limits. The flux contour map represents the intensity of the reactively scattered products as a function of product velocity (u) and scattering angle (θ), and the color bar indicates the flux gradient from high (H) to low (L) intensity.

While this provides strong evidence for the production of **p1**, the formation of other products from the experiment cannot be discounted as the lower energy portion of the $P(E_T)$ may encompass the kinetic energy release of multiple species. The reaction between carbon and acetonitrile features three entrance channels via addition, each without a barrier. First, the carbon atom can add across the carbon−nitrogen triple bond of the cyano group of acetonitrile forming a three-membered cyclic collision complex (**i1**) stabilized by 147 kJ mol^{-1} with respect to the separated reactants. There are a few different pathways to **p1** from **i1**, with the most energetically favorable route involving the three-membered ring opening to a triplet carbene CH_3CCN structure (**i1** → **i2**) over a small 17 kJ mol^{-1} barrier with respect to **i1**, and subsequent hydrogen atom loss from the methyl group (**i2** → **p1**) over a relatively loose exit transition state 7 kJ mol^{-1} above **p1**. Alternate routes from **i1** to the 1-cyanovinyl radical include ring opening to **i4**, ring formation and simultaneous [1,3]-hydrogen shift (**i4** → **i6**), ring opening to an N-terminated structure (**i6** → **i7**), and finally hydrogen atom loss to **p1**. A [1,2]-hydrogen shift can also occur from **i2** to **i6** followed by **p1** formation via hydrogen atom loss. Intermediates **i1** and **i6** are likewise connected through a single transition state with a [1,3]-hydrogen shift from the methyl group to the three-membered ring (**i1** → **i6**). However, these three pathways feature maximum barrier heights, which are 145, 21, and 40 kJ mol^{-1} higher in energy than those for the first path, respectively, suggesting that the **i1** → **i2** → **p1** route is favored. The second entrance channel features carbon atom addition to the carbon of the cyano moiety of acetonitrile, which serves as another pathway to **i4**. The third entrance channel is initiated through carbon-atom addition to the nitrogen of acetonitrile forming **i3** which, aside from leading to the 1-isocyanovinyl product (**p3**) through atomic hydrogen loss, can undergo ring closure forming **i1** and eventually form **p1** through previously discussed pathways. Any other products not shown on the PES lie above the experimental collision energy and cannot be formed in the present study (Figure S2).

Rice−Ramsperger−Kassel−Marcus (RRKM) theory was exploited to calculate the statistical rate constants for each reaction step (Table S1); these rate constants were then utilized to evaluate the branching ratios of the products (Tables S2−S4). Considering initial intermediate populations of 100% at **i1** or **i4** at a collision energy of 25 kJ mol^{-1}, the branching ratios of products **p1**, **p2**/**p2′**, and **p3** are 38%, 16%, and 46%, respectively, with no formation of other products. Conversely, with carbon-atom addition to the nitrogen of acetonitrile, i.e., starting from **i3**, the 1-isocyanovinyl radical (**p3**) is almost exclusively formed, with negligible amounts of **p1** and **p2**/**p2′**. Even without the aid of molecular dynamics simulations to determine the favored entrance channels, **i1** and/or **i4** must be initially populated since **p1** was observed in the experiment. Interestingly, the statistically most likely product to form from the reaction of carbon with acetonitrile regardless of the entrance channel is **p3**. While the experimental data do not provide direct evidence for the

https://doi.org/10.1021/acs.jpca.5c07260
J. Phys. Chem. A 2026, 130, 242−249

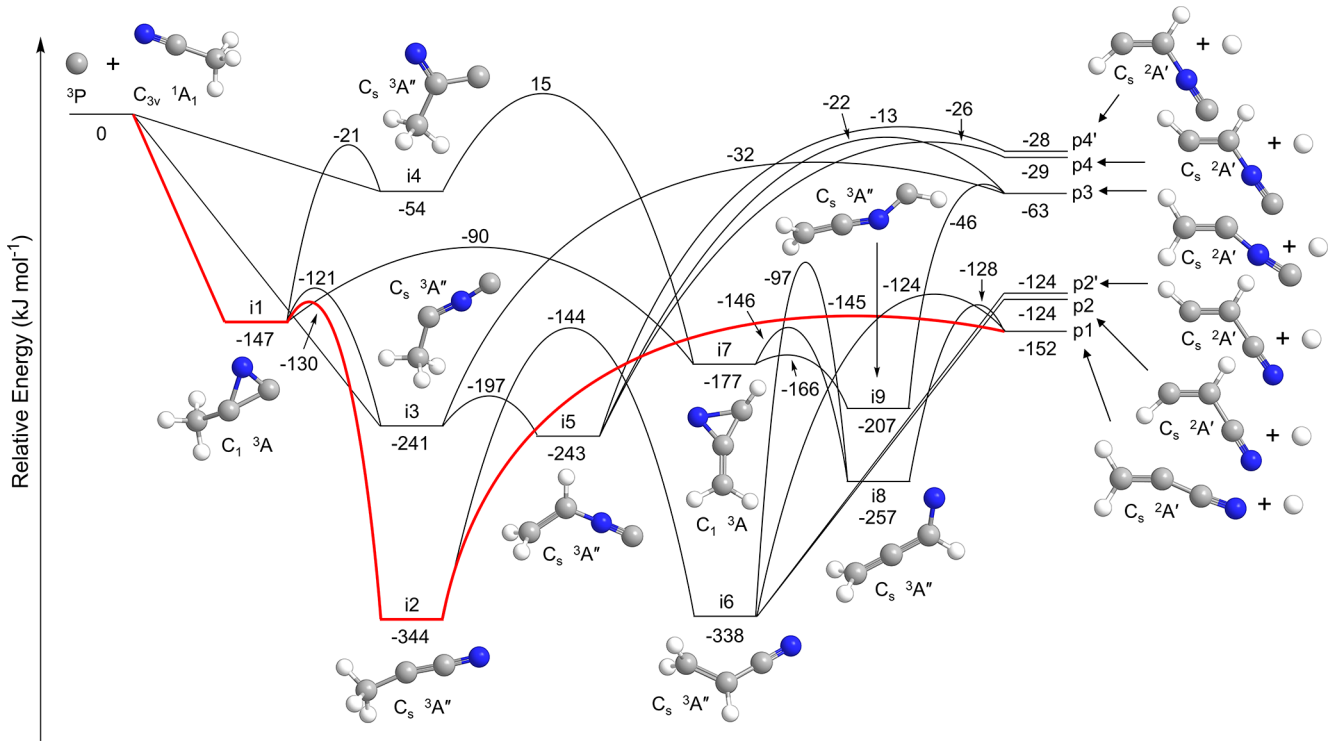

Figure 4. Simplified potential energy surface (PES) for the reaction of ground-state atomic carbon (C, ^{3}P) with acetonitrile (CH_3CN) at the CCSD(T)-F12/cc-pVQZ-F12//ωB97XD/6-311G** + ZPE(ωB97XD/6-311G**) level of theory. Point groups and electronic ground-state term symbols are shown for the reactants, intermediates, and products, and the red lines show the most probable pathway to **p1**. The full PES is shown in Figure S2.

formation of **p3**, it is still possible as the kinetic energy release of **p3** may be cloaked within the lower energy portion of the translational energy distribution (Figure 3a). Overall, our results unequivocally support the barrierless exoergic synthesis of at least the 1-cyanovinyl radical coupled to atomic hydrogen loss.

4. CONCLUSION

In summary, the gas-phase bimolecular reaction of ground-state atomic carbon (C, ^{3}P) with acetonitrile-d_3 (CD_3CN) was explored experimentally under single-collision conditions. These results were combined with high-level computations, revealing the formation of the 1-cyanovinyl radical (D_2CCCN, **p1**) plus atomic deuterium in an overall exoergic reaction. The most likely pathway to **p1** involves carbon atom addition across the nitrile triple bond, ring opening, and unimolecular decomposition via atomic deuterium loss. All entrance channels proceed without a barrier, suggesting that these routes may commence in low-temperature environments such as the cold molecular cloud TMC-1 or the atmosphere of Saturn's moon Titan, thus offering a plausible link to the astronomical observation of the 1-cyanovinyl radical.[14] In these environments, it is possible that the 1-cyanovinyl radical may act as a precursor to larger cyanides, cyano-substituted polycyclic aromatic hydrocarbons (PAHs), or N-heterocycles. Indeed, a study modeling Titan's atmosphere revealed the isovalent 1- and 2-ethynylvinyl radicals (C_4H_3) as building blocks of pyridine (C_5H_5N) from their reactions with the methylene amidogen radical (H_2CN) and stabilization by a third-body collision;[41] it follows that swapping both reactants with their isovalent counterparts, i.e., the reaction of the cyanovinyl radical with the vinyl radical (C_2H_3), should also form pyridine under the low-temperature conditions present on Titan, where pyridine has been detected with Cassini's Plasma Spectrometer (CAPS).[42] Reactions of ethynyl (C_2H),[43,44] cyano (CN),[45] and phenyl (C_6H_5)[46] radicals with methylacetylene (CH_3CCH)—the isovalent counterpart to acetonitrile—have previously been studied; however, unlike reactions of atomic carbon with methylacetylene[18] and acetonitrile, none of these systems produce a substituted vinyl radical. RRKM calculations show that the 1-cyanovinyl radical has more than double the predicted yield from the title reaction compared to its 2-cyanovinyl isomers, which may contribute to why the *E*- and *Z*-2-cyanovinyl radicals have yet to be detected in the interstellar medium. Conversely, the 1-isocyanovinyl radical is predicted to be the major product from the reaction of carbon with acetonitrile at low temperatures, indicating that this species would make a valid target for astronomical surveys of dense molecular clouds like TMC-1. In all, the reaction of ground-state atomic carbon with acetonitrile provides a glimpse into the fundamental carbon−nitrogen chemistry crucial to understanding the chemical processes in deep space.

■ ASSOCIATED CONTENT

Supporting Information

The Supporting Information is available free of charge at https://pubs.acs.org/doi/10.1021/acs.jpca.5c07260.

Comparison of TOFs at different masses (Figure S1), full PES (Figure S2), RRKM rate constants (Table S1), product branching ratios (Tables S2−S4), Cartesian coordinates of all species (Data S1) (PDF)

https://doi.org/10.1021/acs.jpca.5c07260
J. Phys. Chem. A 2026, 130, 242−249

AUTHOR INFORMATION

Corresponding Authors

Alexander M. Mebel − *Department of Chemistry and Biochemistry, Florida International University, Miami, Florida 33199, United States;* orcid.org/0000-0002-7233-3133; Email: mebela@fiu.edu

Ralf I. Kaiser − *Department of Chemistry, University of Hawaii at Manoa, Honolulu, Hawaii 96822, United States;* orcid.org/0000-0002-7233-7206; Email: ralfk@hawaii.edu

Authors

Shane J. Goettl − *Department of Chemistry, University of Hawaii at Manoa, Honolulu, Hawaii 96822, United States;* orcid.org/0000-0003-1796-5725

Ashleigh G. Hartwig − *Department of Chemistry and Biochemistry, Florida International University, Miami, Florida 33199, United States*

Zhenghai Yang − *Department of Chemistry, University of Hawaii at Manoa, Honolulu, Hawaii 96822, United States*

Complete contact information is available at: https://pubs.acs.org/10.1021/acs.jpca.5c07260

Author Contributions

#S.J.G. and A.G.H. contributed equally to this work.

Notes

The authors declare no competing financial interest.

ACKNOWLEDGMENTS

This work was supported by the U.S. Department of Energy, Basic Energy Sciences grant DE-FG02-03ER15411 to the University of Hawaii.

REFERENCES

(1) McKellar, A. Evidence for the molecular origin of some hitherto unidentified interstellar lines. *Publ. Astron. Soc. Pac.* **1940**, *52*, 187.

(2) Turner, B. Detection of interstellar cyanoacetylene. *Astrophys. J.* **1971**, *163*, L35.

(3) Kaifu, N.; Morimoto, M.; Nagane, K.; Akabane, K.; Iguchi, T.; Takagi, K. Detection of interstellar methylamine. *Astrophys. J.* **1974**, *191*, L135.

(4) Godfrey, P.; Brown, R.; Robinson, B.; Sinclair, M. Discovery of interstellar methanimine (formaldimine). *Astrophys. Lett.* **1973**, *13*, 119.

(5) Tielens, A. G. G. M. *The Physics and Chemistry of the Interstellar Medium*; Cambridge University Press, 2005.

(6) Herbst, E. The synthesis of large interstellar molecules. *Int. Rev. Phys. Chem.* **2017**, *36* (2), 287.

(7) Raulin, F.; Brassé, C.; Poch, O.; Coll, P. Prebiotic-like chemistry on Titan. *Chem. Soc. Rev.* **2012**, *41* (16), 5380.

(8) McKay, C. P. Titan as the abode of life. *Life* **2016**, *6* (1), 8.

(9) Woon, D. E. *The Astrochymist*. https://www.astrochymist.org/, 2025.

(10) Snyder, L. E.; Buhl, D. Observations of radio emission from interstellar hydrogen cyanide. *Astrophys. J.* **1971**, *163*, L47.

(11) Solomon, P.; Jefferts, K.; Penzias, A.; Wilson, R. Detection of millimeter emission lines from interstellar methyl cyanide. *Astrophys. J.* **1971**, *168*, L107.

(12) Gardner, F.; Winnewisser, G. The detection of interstellar vinyl cyanide (acrylonitrile). *Astrophys. J.* **1975**, *195*, L127.

(13) Irvine, W. M.; Friberg, P.; Hjalmarson, A.; Ishikawa, S.; Kaifu, N.; Kawaguchi, K.; Madden, S.; Matthews, H.; Ohishi, M.; Saito, S.; Suzuki, H. Identification of the interstellar cyanomethyl radical (CH_2CN) in the molecular clouds TMC-1 and Sagittarius B2. *Astrophys. J.* **1988**, *334*, L107.

(14) Cabezas, C.; Tang, J.; Agúndez, M.; Seiki, K.; Sumiyoshi, Y.; Ohshima, Y.; Tercero, B.; Marcelino, N.; Fuentetaja, R.; de Vicente, P.; Endo, Y.; Cernicharo, J. Laboratory and astronomical discovery of the cyanovinyl radical H_2CCCN. *Astron. Astrophys.* **2023**, *676*, L5.

(15) Hickson, K. M.; Loison, J.-C.; Wakelam, V. Kinetic study of the gas-phase $C(^3P)$ + CH_3CN reaction at low temperatures: Rate constants, H-atom product yields, and astrochemical implications. *ACS Earth Space Chem.* **2021**, *5* (4), 824.

(16) Johansen, S. L.; Martin-Drumel, M.-A.; Crabtree, K. N. Rotational spectrum of the β-cyanovinyl radical: A possible astrophysical N-heterocycle precursor. *J. Phys. Chem. A* **2019**, *123* (24), 5171.

(17) Sun, J.; Wang, R.; Wang, B. Theoretical study on the gas phase reaction of acrylonitrile with a hydroxyl radical. *Phys. Chem. Chem. Phys.* **2011**, *13* (37), 16585.

(18) Kaiser, R. I.; Stranges, D.; Lee, Y. T.; Suits, A. G. Crossed-beam reaction of carbon atoms with hydrocarbon molecules. II. Chemical dynamics of n-C_4H_3 formation from reaction of $C(^3P_j)$ with methylacetylene, CH_3CCH (X^1A_1). *J. Chem. Phys.* **1996**, *105* (19), 8721.

(19) Kaiser, R. I.; Mebel, A. M.; Lee, Y. T.; Chang, A. H. H. Unimolecular decomposition of chemically activated triplet C_4HD_3 complexes: A combined crossed-beam and ab initio study. *J. Chem. Phys.* **2001**, *115* (11), 5117.

(20) Kaiser, R. I.; Mebel, A. M.; Chang, A. H. H.; Lin, S. H.; Lee, Y. T. Crossed-beam reaction of carbon atoms with hydrocarbon molecules. V. Chemical dynamics of n-C_4H_3 formation from reaction of $C(^3P_j)$ with allene, $H_2CCCH_2(X^1A_1)$. *J. Chem. Phys.* **1999**, *110* (21), 10330.

(21) Goldreich, P.; Kwan, J. Molecular Clouds. *Astrophys. J.* **1974**, *189*, 441.

(22) Mitchell, J. L.; Lora, J. M. The climate of Titan. *Annu. Rev. Earth Planet. Sci.* **2016**, *44* (1), 353.

(23) Gu, X.; Guo, Y.; Kaiser, R. I. Mass spectrum of the butadiynyl radical (C_4H; $X^2\Sigma^+$). *Int. J. Mass Spectrom.* **2005**, *246* (1−3), 29.

(24) Proch, D.; Trickl, T. A high-intensity multi-purpose piezoelectric pulsed molecular beam source. *Rev. Sci. Instrum.* **1989**, *60* (4), 713.

(25) Daly, N. R. Scintillation type mass spectrometer ion detector. *Rev. Sci. Instrum.* **1960**, *31* (3), 264.

(26) Vernon, M. F. *Molecular beam scattering*. Ph.D. Dissertation; University of California at Berkeley: Berkeley, CA, 1983.

(27) Weiss, P. S. *Reaction dynamics of electronically excited alkali atoms with simple molecules*. Ph.D. Dissertation; University of California at Berkeley: Berkeley, CA, 1985.

(28) Kaiser, R. I.; Ochsenfeld, C.; Stranges, D.; Head-Gordon, M.; Lee, Y. T. Combined crossed molecular beams and ab initio investigation of the formation of carbon-bearing molecules in the interstellar medium via neutral−neutral reactions. *Faraday Discuss.* **1998**, *109*, 183−204.

(29) Frisch, M. J.; Trucks, G. W.; Schlegel, H. B.; Scuseria, G. E.; Robb, M. A.; Cheeseman, J. R.; Scalmani, G.; Barone, V.; Petersson, G. A.; Nakatsuji, H., et al. *Gaussian 16, Revision C.01*; Gaussian Inc.: Wallingford, CT, 2016; http://www.gaussian.com.

(30) Halsey-Moore, C.; Jena, P.; McLeskey, J. T. Tuning range-separated DFT functionals for modeling the peak absorption of MEH-PPV polymer in various solvents. *Comput. Theor. Chem.* **2019**, *1162*, 112506.

(31) Chai, J.-D.; Head-Gordon, M. Long-range corrected hybrid density functionals with damped atom−atom dispersion corrections. *Phys. Chem. Chem. Phys.* **2008**, *10* (44), 6615.

(32) Werner, H. J.; Knowles, P. J.; Knizia, G.; Manby, F. R.; Schütz, M.; Celani, P.; Györffy, W.; Kats, D.; Korona, T.; Lindh, R., et al. *MOLPRO, a Package Of Ab Initio Programs Version 2021.2*; University of Cardiff: Cardiff, UK, 2021. http://www.molpro.net.

(33) Zhang, J.; Valeev, E. F. Prediction of reaction barriers and thermochemical properties with explicitly correlated coupled-cluster methods: A basis set assessment. *J. Chem. Theory Comput.* **2012**, *8* (9), 3175.

(34) Garrett, B. C.; Truhlar, D. G. *Encyclopedia of Computational Chemistry*; Schleyer, P. v. R.; Allinger, N. L.; Clark, T.; Gastreiger, J.; Kollman, P. A.; Schaefer, H. F.; Schreiner, P. R., Eds.; John Wiley & Sons: Hoboken, NJ, USA, 1998; Vol. 5, p 3094.
(35) Di Giacomo, F. A short account of RRKM theory of unimolecular reactions and of Marcus theory of electron transfer in a historical perspective. *J. Chem. Educ.* **2015**, *92* (3), 476.
(36) Cleaves, H. J. *Encyclopedia of Astrobiology*; Gargaud, M.; Amils, R.; Quintanilla, J. C.; Cleaves, H. J.; Irvine, W. M.; Pinti, D. L.; Viso, M., Eds.; Springer: Berlin, Heidelberg, 2011, p 1459.
(37) Kislov, V. V.; Nguyen, T. L.; Mebel, A. M.; Lin, S. H.; Smith, S. C. Photodissociation of benzene under collision-free conditions: An ab initio /Rice−Ramsperger−Kassel−Marcus study. *J. Chem. Phys.* **2004**, *120* (15), 7008.
(38) He, C.; Zhao, L.; Thomas, A. M.; Morozov, A. N.; Mebel, A. M.; Kaiser, R. I. Elucidating the chemical dynamics of the elementary reactions of the 1-propynyl radical (CH_3CC; X^2A_1) with methylacetylene (H_3CCCH; X^1A_1) and allene (H_2CCCH_2; X^1A_1). *J. Phys. Chem. A* **2019**, *123* (26), 5446.
(39) Herschbach, D. R. Reactive collisions in crossed molecular beams. *Discuss. Faraday Soc.* **1962**, *33*, 149.
(40) Yang, Z.; He, C.; Goettl, S. J.; Mebel, A. M.; Velloso, P. F. G.; Alves, M. O.; Galvão, B. R. L.; Loison, J.-C.; Hickson, K. M.; Dobrijevic, M.; Li, X.; Kaiser, R. I. Low-temperature formation of pyridine and (iso)quinoline via neutral−neutral reactions. *Nat. Astron.* **2024**, *8* (7), 856.
(41) Laskin, J.; Lifshitz, C. Kinetic energy release distributions in mass spectrometry. *J. Mass Spectrom.* **2001**, *36* (5), 459−478.
(42) Ali, A.; Sittler, E. C.; Chornay, D.; Rowe, B. R.; Puzzarini, C. Organic chemistry in Titan's upper atmosphere and its astrobiological consequences: I. Views towards Cassini plasma spectrometer (CAPS) and ion neutral mass spectrometer (INMS) experiments in space. *Planet. Space Sci.* **2015**, *109-110*, 46−63.
(43) Stahl, F.; Schleyer, P. v. R.; Bettinger, H. F.; Kaiser, R. I.; Lee, Y. T.; Schaefer III, H. F. Reaction of the ethynyl radical, C_2H, with methylacetylene, CH_3CCH, under single collision conditions: Implications for astrochemistry. *J. Chem. Phys.* **2001**, *114* (8), 3476−3487.
(44) Stahl, F.; Schleyer, P. v. R.; Schaefer III, H. F.; Kaiser, R. I. Reactions of ethynyl radicals as a source of C_4 and C_5 hydrocarbons in Titan's atmosphere. *Planet. Space Sci.* **2002**, *50*, 685−692.
(45) Huang, L. C. L.; Balucani, N.; Lee, Y. T.; Kaiser, R. I.; Osamura, Y. Crossed beam reaction of the cyano radical, $CN(X^2\Sigma^+)$, with methylacetylene, $CH_3CCH(X^1A_1)$: Observation of cyanopropyne, $CH_3CCCN(X^1A_1)$, and cyanoallene, $H_2CCCHCN(X^1A')$. *J. Chem. Phys.* **1999**, *111* (7), 2857.
(46) Gu, X.; Kaiser, R. I. Reaction dynamics of phenyl radicals in extreme environments: A crossed molecular beam study. *Acc. Chem. Res.* **2009**, *42* (2), 290.

https://doi.org/10.1021/acs.jpca.5c07260
J. Phys. Chem. A 2026, 130, 242−249